Supporting Information

Exfoliated 2D Lepidocrocite Titanium Oxide Nanosheets for High Sulfur Content Cathodes with Highly Stable Li–S Battery Performance

Sharad B. Patil,[†,§] Hyeon Jin Kim,[‡,§] Hyung-Kyu Lim,[‡,∥] Seung Mi Oh,[†] Jiheon Kim,[‡] Jaeho Shin,[⊥] Hyungjun Kim,[‡,∥] Jang Wook Choi,[⊥,] and Seong-Ju Hwang[†,*]*

[†] Department of Chemistry and Nanoscience, Ewha Womans University, Seoul 03760, Republic of Korea

[‡] Graduate School of Energy, Environment, Water, and Sustainability (EEWS), Korea Advanced Institute of Science and Technology (KAIST), 291 Daehak-ro, Yuseong-gu, Daejeon 34141, Republic of Korea

[∥] Department of Chemistry, Korea Advanced Institute of Science and Technology (KAIST), Daejeon 34141, Republic of Korea

[⊥] School of Chemical and Biological Engineering and Institute of Chemical Processes, Seoul National University, 1 Gwanak-ro, Gwanak-gu, Seoul 08826, Republic of Korea

Corresponding Author

* jangwookchoi@snu.ac.kr (J.W.C.)

* hwangsju@ewha.ac.kr (S.-J.H.)

Methods

Synthesis of exfoliated 2D titanium oxide nanosheets: The pristine LT ($Cs_{0.67}Ti_{1.83}\square_{0.17}O_4$) and TT ($Na_2Ti_3O_7$) materials were prepared by a conventional solid-state reaction with Cs_2CO_3/K_2CO_3 and TiO_2 precursors at 800–900 °C, as reported previously.[1–3] Their protonated derivatives ($H_{0.67}Ti_{1.83}\square_{0.17}O_4$ and $H_2Ti_3O_7$) were obtained by the reaction of the pristine materials with excess 1 M HCl aqueous solution at room temperature for 24 h. The exfoliation of LT was achieved by intercalation of tetrabutylammonium ions into the protonated LT derivative, yielding the aqueous colloidal suspension of LT nanosheets.[1] Similarly, the exfoliated TT nanosheets were attained by the sequential intercalation of methylammonium and propylammonium into the protonated TT derivative.[2] Prior to the loading of sulfur, the obtained colloidal suspensions of titanium oxide nanosheets were dialyzed with distilled water to completely remove excess tetrabutylammonium and propylammonium ions.

Synthesis of hollow TiO_2 microspheres: Hollow TiO_2 microsphere was prepared by solvothermal reaction of tetra-*n*-butyl titanium oxide, acetylacetone, and isopropyl alcohol at 200 °C for 8 h, as reported previously.[4] The product was separated by centrifugation, washed with ethanol several times, and dried at 60 °C overnight.

Synthesis of 2D titanium oxide nanosheet–sulfur nanocomposites: An aqueous solution of $Na_2S{\cdot}9H_2O$ (Sigma-Aldrich) and Na_2SO_3 (Sigma-Aldrich) was added into the aqueous colloidal suspensions of LT or TT nanosheets under vigorous stirring. Then, aqueous 1 M HCl solution and PVP were simultaneously added dropwise into the resulting colloidal suspensions. Next, the solution baths were ultrasonicated for 0.5 h. The products were separated by centrifugation, washed with distilled water for several times, and vacuum-dried at 60 °C for 12 h. The obtained products were heated at 150 °C for 5 h under Ar flow. Two kinds of the **LTS** nanocomposites were prepared with the sulfur contents of 88 and 80 wt%.

Also, two kinds of sulfur contents of 90 and 80 wt% were employed for the synthesis of **TTS** nanocomposites. The control **HTS** and **ATS** nanocomposites with the sulfur content of 80 wt% were prepared by the same synthetic procedure.

Synthesis of Li_2S_n: The reference Li_2S_n was prepared by reacting elemental sulfur with 1 M THF solution of lithium triethylborohydride in a molar ratio of 2.75:1 in an Ar-filled glovebox.[5] After the reaction, the precipitated yellow powder of Li_2S_n was obtained by drying the resulting solution under vacuum. The obtained yellow product was washed with toluene and vacuum-dried.

Synthesis of LT–Li_2S_n, TT–Li_2S_n, HT–Li_2S_n, and AT–Li_2S_n: The LT and TT nanosheets were restored from the corresponding colloidal suspensions by freeze-drying and vacuum-drying at 150 °C for 12 h. 0.2 mmol of LT, TT, HT, and AT were mixed with 0.6 mmol of Li_2S_n in THF (Sigma-Aldrich) in an Ar-filled glovebox. The obtained mixtures were stirred for 6 h. The products were separated by centrifugation and dried under vacuum overnight.

Synthesis of activated carbon–sulfur composite: Activated carbon and sulfur were mechanically mixed and heat-treated at 158 °C for 12 h.

Characterization: The crystal structures of the nanocomposites were investigated by carrying out powder X-ray diffraction (XRD) analysis at room temperature using a Rigaku diffractometer with Ni-filtered Cu Kα radiation. The Rietveld refinement for the collected XRD patterns was performed using the GSAS[6,7] program package. During the Rietveld refinement, the peak profiles were simulated using the pseudo-Voigt function and the background was defined with 16 term shifted Chebyschev function. The occupancy parameters of all the atoms were kept fixed at the nominal compositions. The scale factor, background, zero-angle shift, lattice parameters, and peak profiles were refined simultaneously in the initial refinements. The isotropic thermal parameters and positional coordinates were set as variables in the last step of refinements. The sulfur contents of the

nanocomposites were determined by carrying out thermogravimetric (TG) analysis using TA Instruments SDT Q600. TG curves were collected at a rate of 5 °C min^{-1} under N_2 flow. The field emission-scanning electron microscopy (FE-SEM) and transmission electron microscopy (TEM) micrographs were attained using Jeol JSM-6700F and Jeol JEM-2100F electron microscopes, respectively. The energy dispersive spectrometry (EDS)–elemental maps were recorded with an energy-dispersive X-ray spectrometer equipped in the FE-SEM machine. NH_3-temperature programmed desorption (TPD) measurements were carried out using AutoChem II 2920 (Micrometrics). 40 mg of each sample was heated at 300 °C under He flow. NH_3 adsorption was processed after samples cooled down to 100 °C. NH_3 desorption measurements were carried out by heating the samples to 800 °C with a heating rate of 10 °C min^{-1}. Ti K-edge X-ray absorption near-edge structure (XANES) spectra were collected at extended X-ray absorption fine structure (EXAFS) facility installed in the beamline 10C at the Pohang Accelerator Laboratory (PAL, Pohang, Korea). The XANES data were collected in transmission mode at room temperature. The energy was calibrated by simultaneously measuring the reference spectrum of TiO_2. The chemical interaction of lithium polysulfides (LiPSs) with titanium oxides was investigated by carrying out K-alpha X-ray photoelectron spectroscopy (XPS) analysis (Thermo Scientific Inc., U.K). All the measured XPS data were reproduced with Gaussian–Lorentzian functions and Shirley-type background with the help of the XPSPEAK software. The S 2p spectra were fit with spin-orbit doublets of S $2p_{3/2}$ and S $2p_{1/2}$ components with an energy gap of 1.18 eV and peak area ratio of 2:1 with identical full-width-at-half-maximum (FWHM).

Electrochemical Measurement: Electrochemical properties of titanium oxide–sulfur nanocomposites were evaluated by fabricating CR2032-type coin cells. For this, slurries were prepared by dispersing active materials, Super P, and poly(vinylidene fluoride) (PVDF, MW = 560,000, Aldrich) in N-methyl-2-pyrrolidone (NMP, Junsei Chemical) in a mass ratio of

75:15:10. Each slurry was then cast onto an aluminum foil current collector (20 μm, Hohsen, Japan) using the doctor blade technique, followed by a drying step in a convection oven at 60 °C overnight. The dried samples were punched into 12 pi (1.13 cm^2) circular discs. Each coin cell consists of a cathode, a Li metal foil counter electrode (as both counter and reference electrodes), and a polypropylene separator (Celgard 2400). For the electrolyte, 1 M lithium bis(trifluoromethane)sulfonamide (LiTFSI, Aldrich) and 2 wt% of lithium nitrate ($LiNO_3$, Aldrich) were thoroughly dissolved in a solvent mixture of tetraethylene glycol dimethyl ether (TEGDME, Aldrich) and 1,3-dioxolane (DIOX, Aldrich) (0.33:0.67 in a volume ratio). All the processes were conducted inside an Ar-filled glove box and 40 μL of the electrolyte (22.4 g L^{-1}) was added to each cell. The WBCS 3000 (Wonatech, Korea) battery cycler was used for testing of the fabricated cells under the galvanostatic discharge–charge mode in the potential range of 1.7–2.7 V vs. Li/Li^+. The sulfur loading in the employed sulfur cathodes was 0.8 mg cm^{-2}. All of the specific capacities were calculated based on the mass of sulfur only. The current density in the precycling was 50 mA g^{-1}, and was increased to 1000 mA g^{-1} in the subsequent cycles. The electrodes for ex-situ XPS analysis were discharged at 50 mA g^{-1}.

DFT calculations: We used the Vienna Ab-initio Simulation Package (VASP) software with the exchange-correlation function of Perdew-Burke-Ernzerhof (PBE).[8,9] The electron–ion interaction was considered in the form of the projector-augmented-wave (PAW) method with a plane wave up to energy of 400 eV. The surface models based on the 2×3 supercell of lepidocrocite titanium oxide (ICSD:202181) combined with a 20 Å vacuum layer were fully minimized under a gamma centered k-point grid of (4×3×1). A dipole correction scheme was adopted to electrostatically isolate the surface model from periodic images.

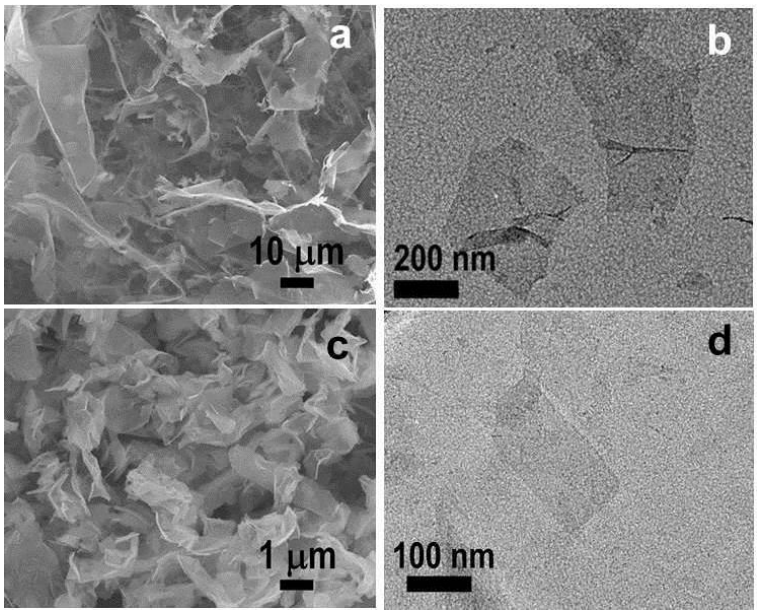

Figure S1. FE-SEM and TEM images of exfoliated (a,b) LT nanosheets and (c,d) TT nanosheets.

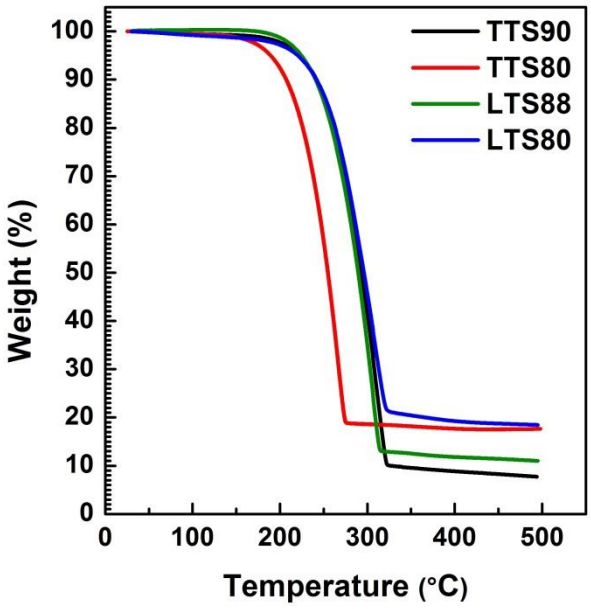

Figure S2. TG curves of the layered titanium oxide–sulfur nanocomposites.

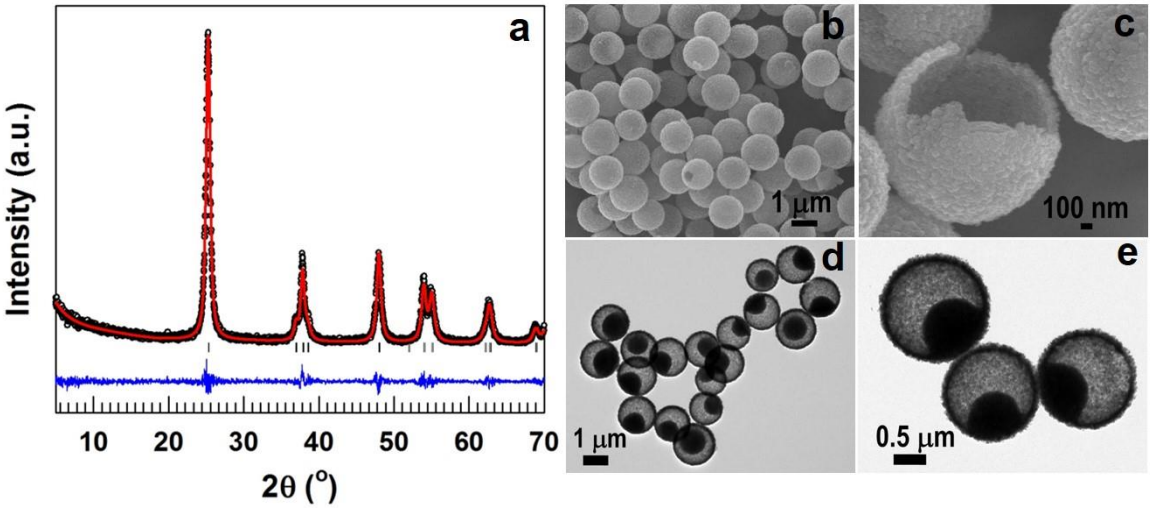

Figure S3. (a) Powder XRD pattern of the HT microspheres. The empty circles (o) represent the observed, red line represents the fit obtained through Rietveld refinement, and blue line represents difference between the observed data and the refinement. Vertical lines (|) represent the positions of Bragg reflections corresponding to the anatase phase of TiO_2 (space group: $I4_1/amd$). (b,c) FE-SEM and (d,e) TEM images of HT microspheres.

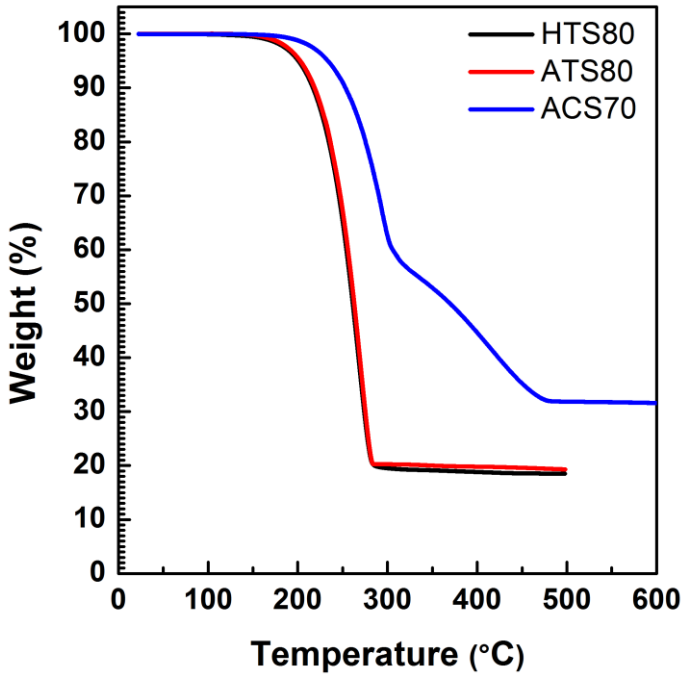

Figure S4. TG curves of the control samples **HTS80**, **ATS80**, and **ACS70**.

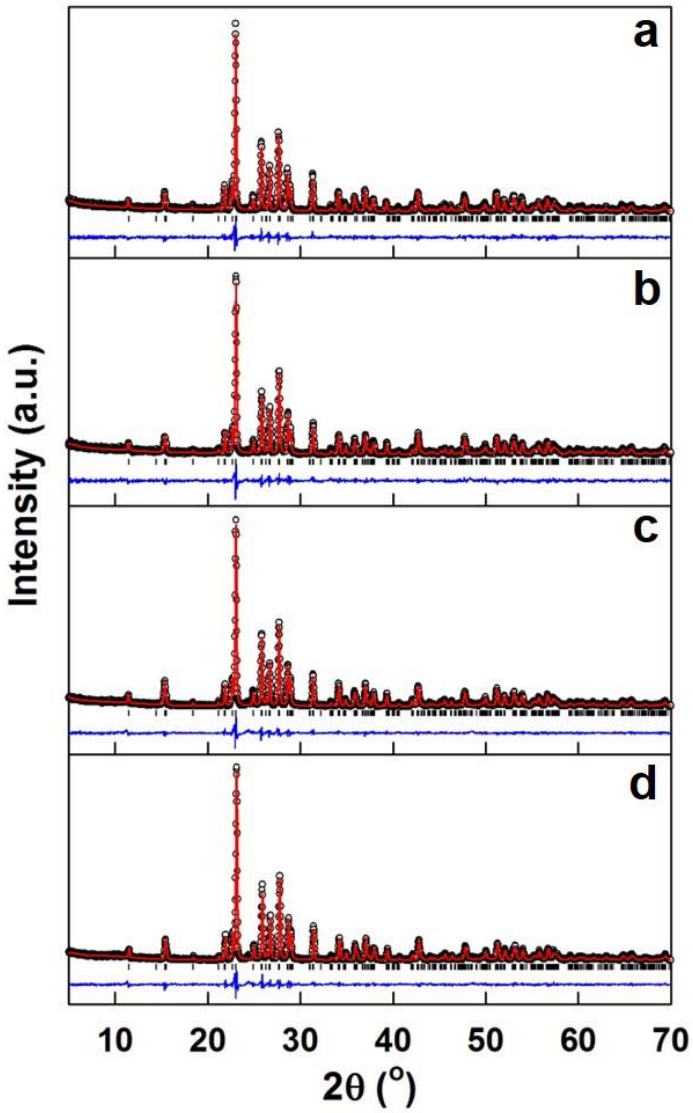

Figure S5. Powder XRD patterns of (a) **LTS88**, (b) **LTS80**, (c) **TTS90**, and (d) **TTS80** nanocomposites. The open circles, red lines, and blue lines represent the observed XRD and calculated XRD patterns, and the difference between them, respectively. Vertical lines (|) represent the positions of Bragg reflections corresponding to the orthorhombic phase of elemental sulfur (space group: Fddd).

Table S1: Refined structural parameters and fitting factors for titanium oxide–sulfur nanocomposites.

		LTS88	**LTS80**	**TTS90**	**TTS80**	**HTS80**	**ATS80**
Sulfur	a (Å)	10.4677	10.4810	10.4791	10.4820	10.4785	10.4814
	b (Å)	12.8726	12.8894	12.8861	12.8895	12.8847	12.8899
	c (Å)	24.4864	24.5160	24.5141	24.5208	24.5082	24.5184
	V ($Å^3$)	3299.45	3311.94	3310.24	3312.95	3308.89	3312.54
	ρ (g cm^{-3})	2.059	2.056	2.035	2.077	2.077	2.260
TiO_2	a (Å)					3.7953	3.7834
	b (Å)					3.7953	3.7834
	c (Å)	-	-	-	-	9.5200	9.5088
	V ($Å^3$)					137.13	136.11
	ρ (g cm^{-3})					3.654	3.899
R_{wp} (%)		13.72	14.03	12.24	11.93	12.93	13.12
R_{exp} (%)		7.90	7.97	6.82	6.70	10.97	7.32
χ^2		3.02	3.10	3.22	3.17	1.39	3.21
R_p (%)		10.61	10.68	9.21	8.96	9.86	9.97
R_F (%)		8.9	9.41	6.16	6.83	7.26	5.00

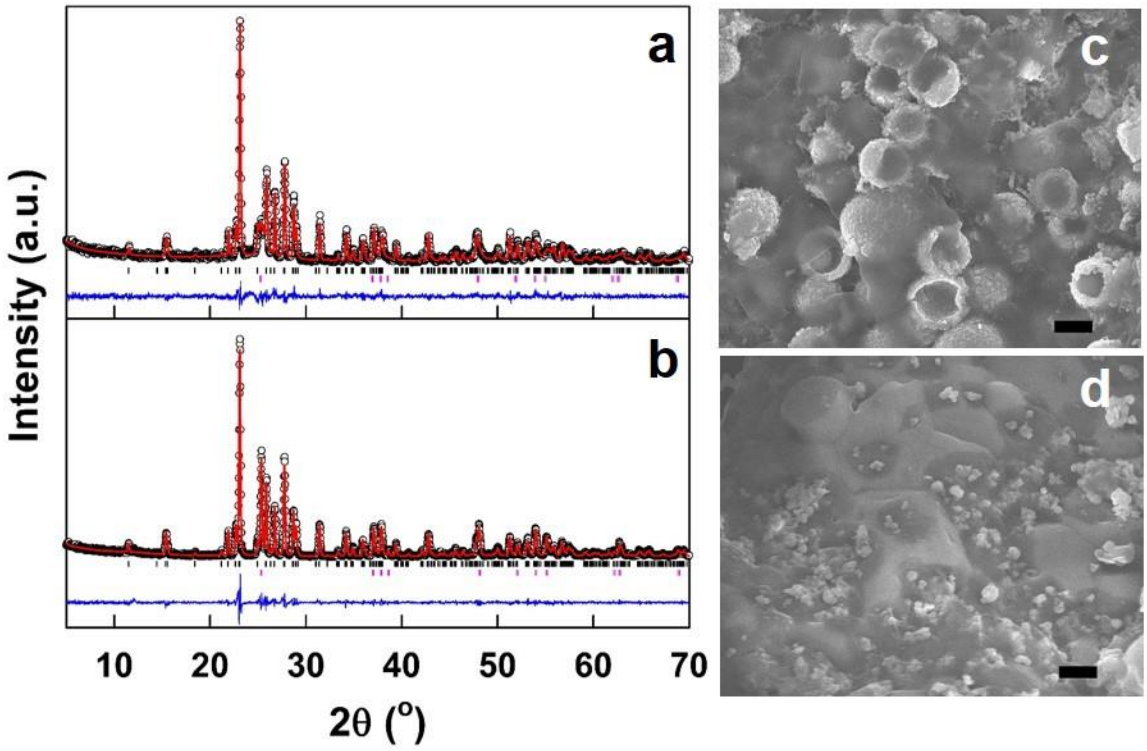

Figure S6. Powder XRD patterns and FE-SEM micrographs of (a,c) **HTS80** and (b,d) **ATS80**, respectively. In the powder XRD patterns, the empty circles (o) represent the observed, red line represents the fit obtained through Rietveld refinement, and blue line represents difference between the observed data and the refinement. Vertical black (|) and pink (|) lines represent the positions of Bragg reflections corresponding to the orthorhombic phase of elemental sulfur (space group: Fddd) and the anatase phase of TiO_2 (space group: $I4_1/amd$), respectively. Scale bars, 1 μm (c,d).

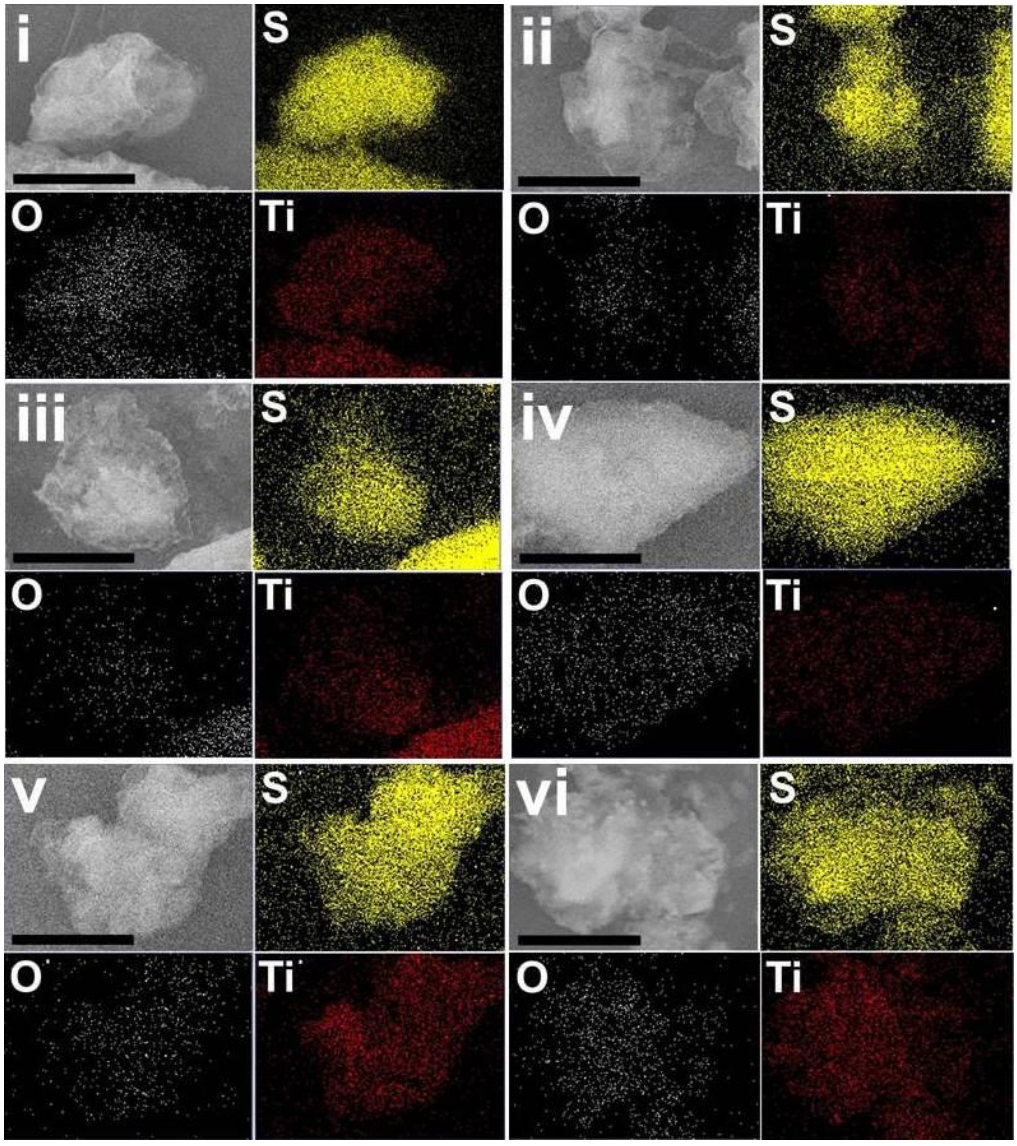

Figure S7. EDS–elemental maps of (i) **LTS80**, (ii) **LTS88**, (iii) **TTS80**, (iv) **TTS90**, and the control samples (v) **HTS80** and (vi) **ATS80**. Scale bars, 6 μm.

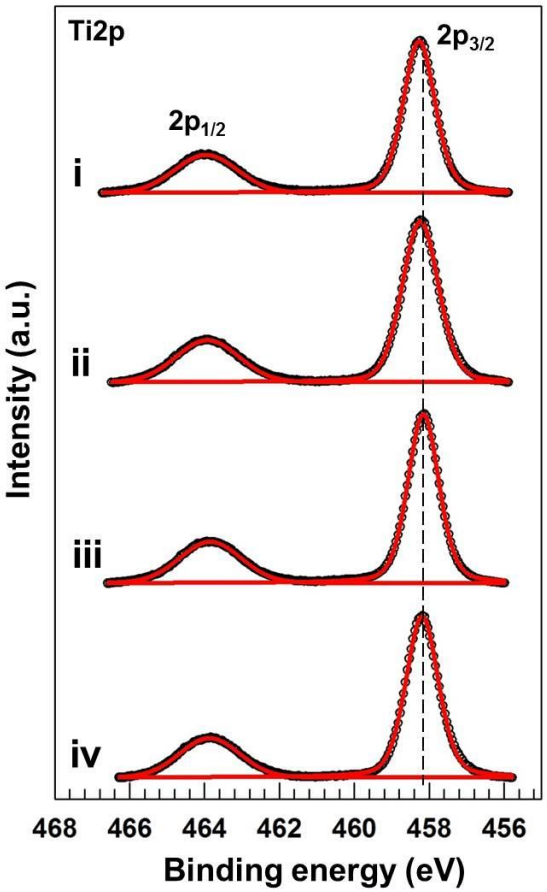

Figure S8. Ti 2p XPS data of (i) HT, (ii) HT–Li_2S_n, (iii) AT, and (iv) AT–Li_2S_n.

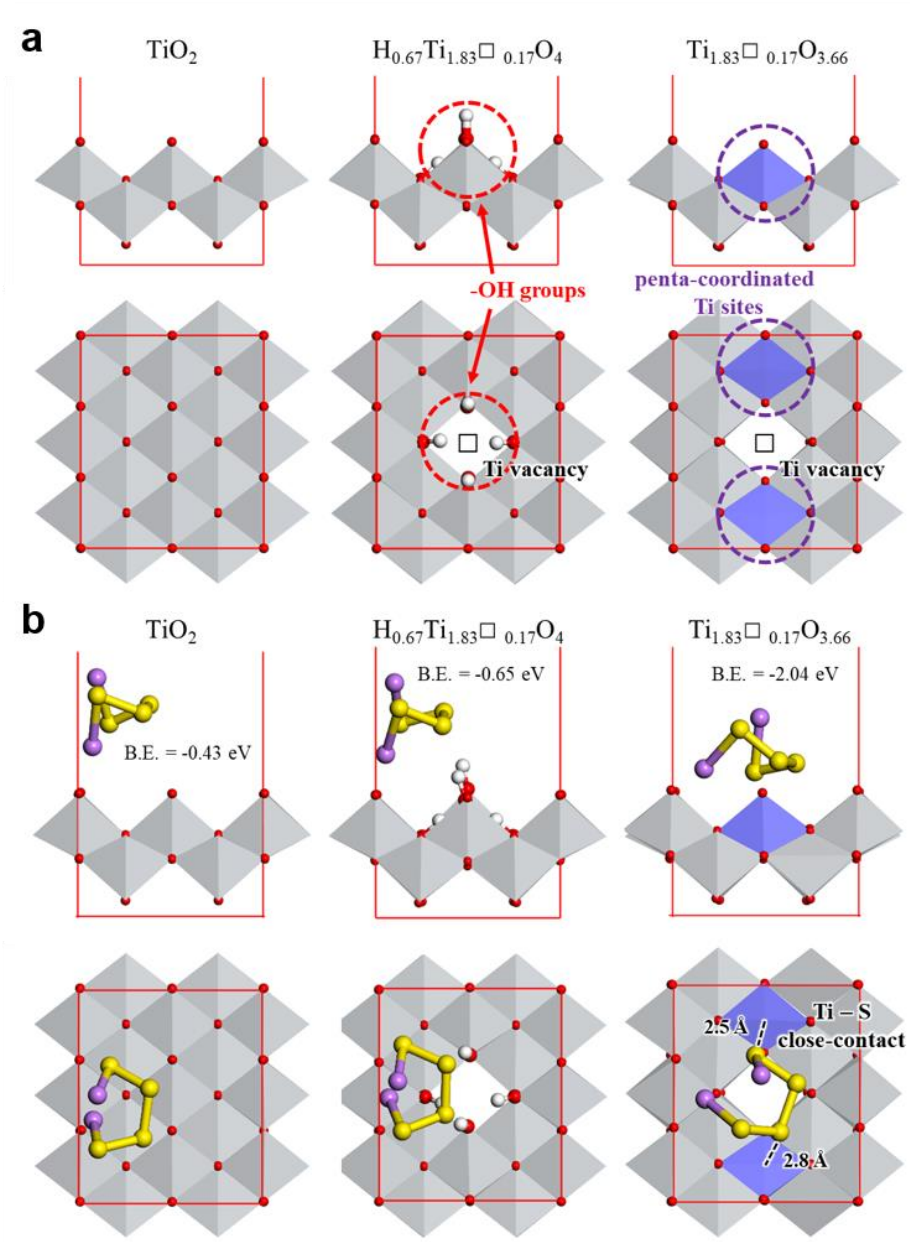

Figure S9. (a) 3 types of surface structures used in density functional theory (DFT) calculations. (b) Li_2S_4 adsorbed surface structures and binding energies.

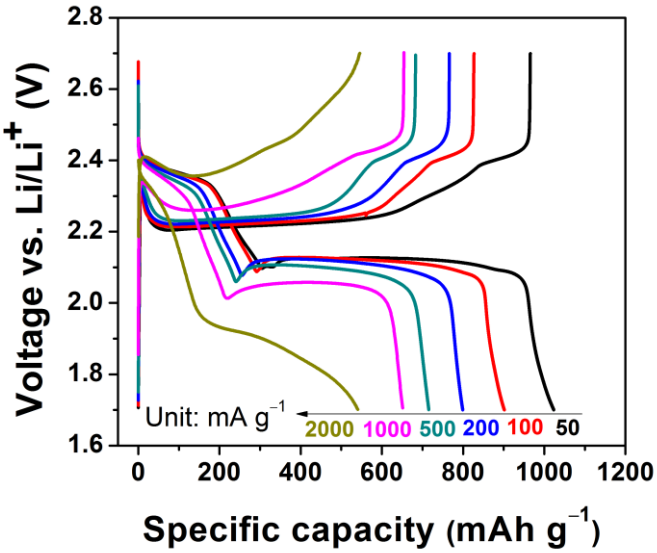

Figure S10. Rate performance of **LTS80** corresponding charge–discharge profiles.

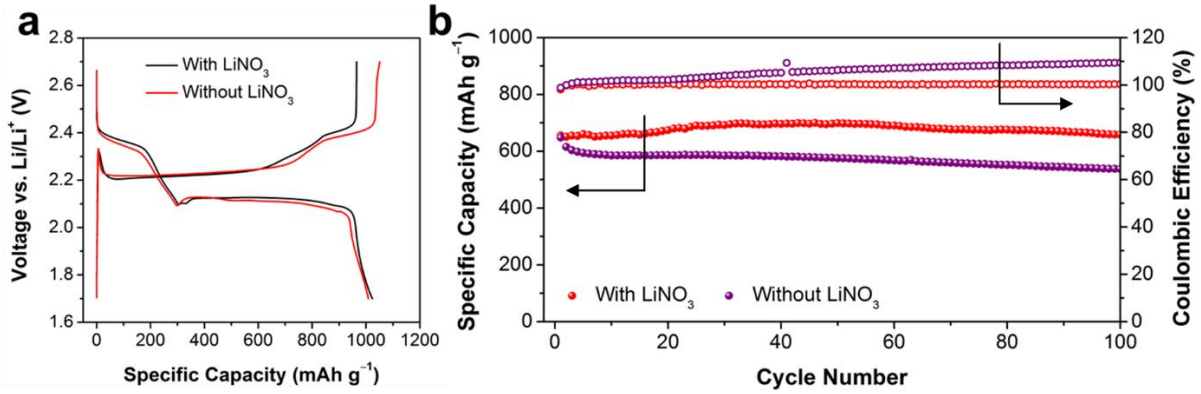

Figure S11. (a) The first discharge–charge profiles and (b) cycling performance of **LTS80** with and without $LiNO_3$ additive.

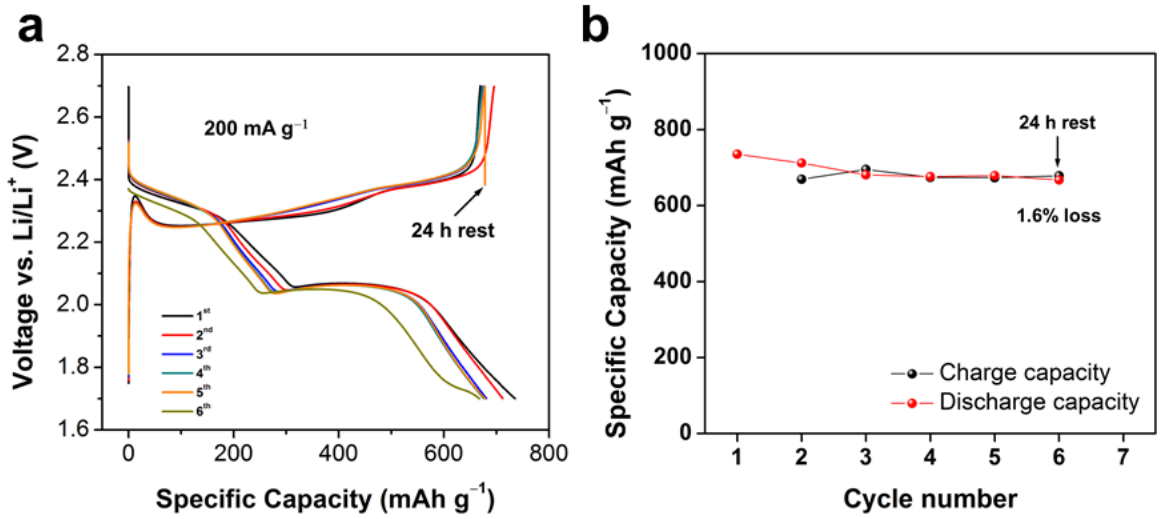

Figure S12. (a) Discharge-charge profiles and (b) cycling performance of **LTS80** at 200 mA g^{-1}. At the 5th fully charge stage, the cell was rested for 24 h, followed by discharging. The percentage of the capacity loss was calculated based on [(5th charge capacity – 6th discharge capacity) / 5th charge capacity] * 100.

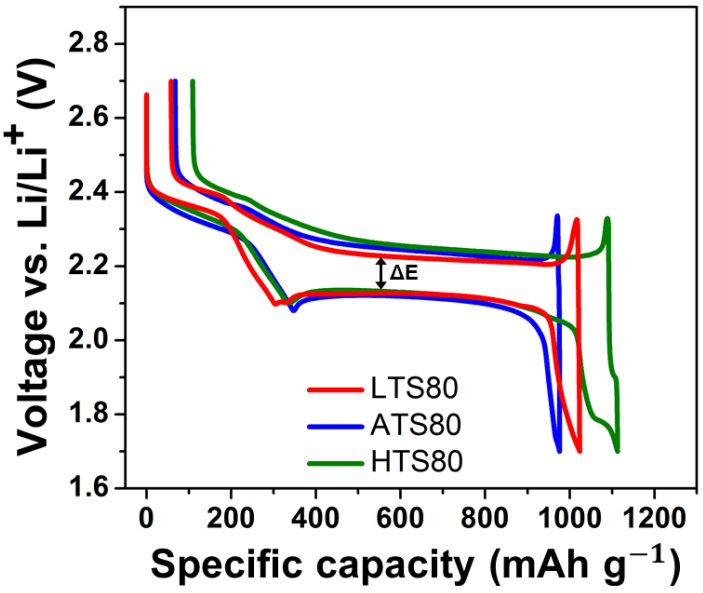

Figure S13. The first discharge–charge profiles of **LTS80**, **ATS80**, and **HTS80** at 50 mA g^{-1}.

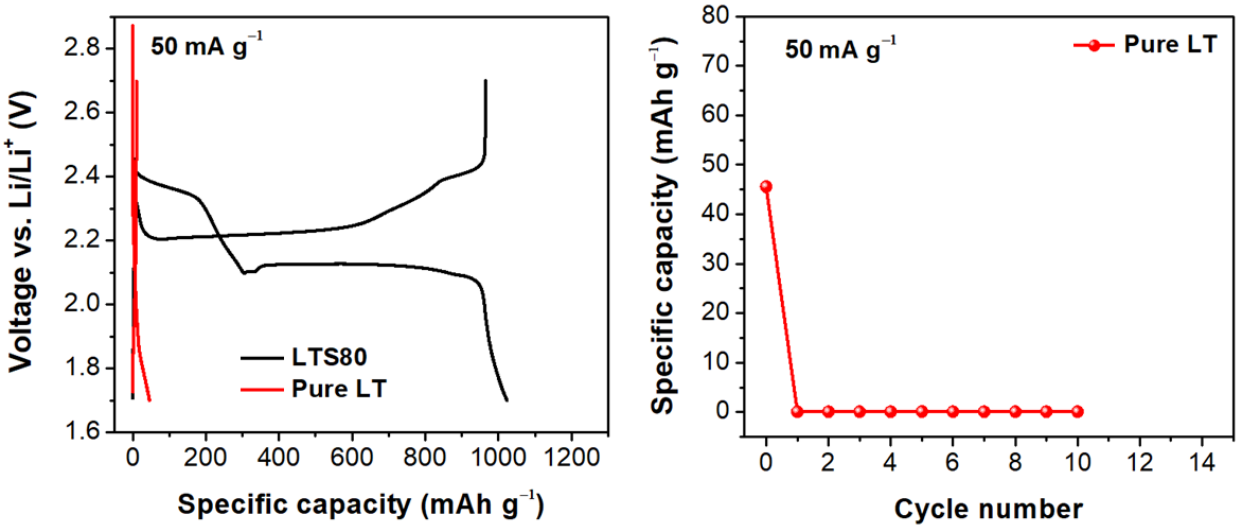

Figure S14. The first discharge–charge profiles with pure LT nanosheets (left) and their cycling performance (right).

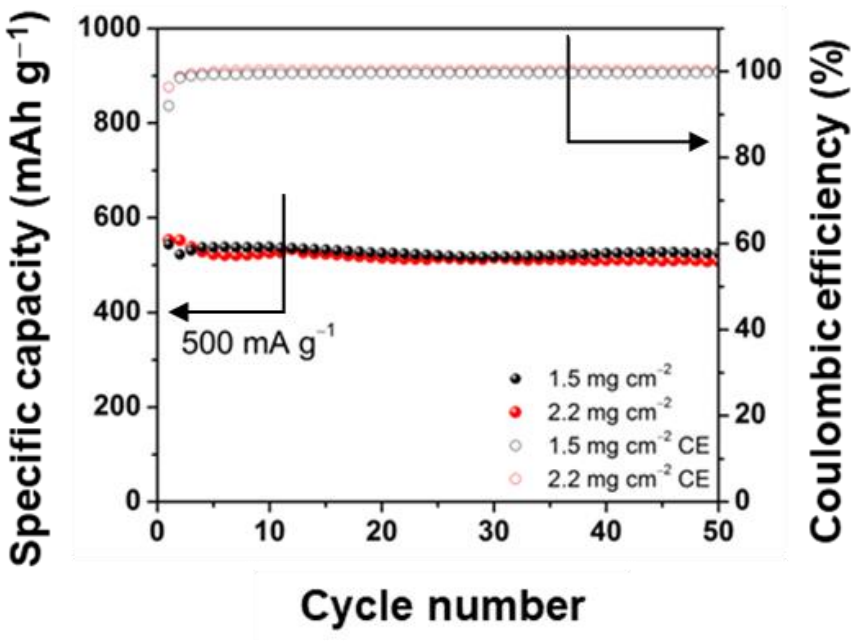

Figure S15. Cycling performance and CEs of **LTS80** with loadings of 1.5 and 2.2 mg cm^{-2} at 500 mA g^{-1}.

Table S2: The comparison of electrochemical performance between the current work and other previous ones employing metal oxide-sulfur composites.

Material	Sulfur content (wt%)	Initial discharge capacity	Capacity retention				Ref
		Capacity (mAh g_s^{-1})	Current density (mA g^{-1})	Cycles	Retention rate (%)	Voltage window (V ver. Li/Li^+)	
Lepidocrocite titanium oxide/S*	**80**	**1024**	**1000**	**300**	**82.3**	**1.7 ~ 2.7**	**This work**
ACS70*	**70**	**1189**	**1000**	**100**	**68.8**	**1.7 ~ 2.7**	**This work**
SCM/α-TiO_2/S	48	1201	1672	200	73	1.5 ~ 2.8	10
H_2-reduced TiO_{2-x}/S	45	1250	335	200	81	1.8 ~ 2.6	11
S/TiO_2 yolk shell	71	~1030	836.5	500	81	1.7 ~ 2.6	12
75S/MnO_2	75	1300	335	200	92	1.8 ~ 3.0	13
Ti_4O_7/S-60	60	1070	3350	500	~70	1.7 ~ 3.0	5
S/V_2O_5–graphene	75	1205	837.5	150	76	1.8 ~ 3.0	14
S/VO_2–graphene	75	1180	837.5	150	74	1.8 ~ 3.0	14
S/Co_3O_4–graphene	75	1141	837.5	250	15	1.8 ~ 3.0	14
S/PAN/$Mg_{0.6}Ni_{0.4}O$	39	1223	167.2	100	~99	1.0 ~ 3.0	15
C/S/mesoporous silica	60	960	334.4	40	67.7	1.5 ~ 3.0	16
NMC/10La_2O_3/S	60	1241	1675	100	76.6	1.5 ~ 3.0	17
ITO–carbon hybrid nanofiber	-	1279	334.6	300	88	1.7 ~ 2.6	18
MCM/Nb_2O_5/S	60	1289	837.5	200	72	1.5 ~ 3.0	19

*Initial capacity was calculated based on the mass of sulfur only.

Table S3: The comparison of energy density between the **LTS80** and previous standard carbon containing sulfur composites.

Material	**Sulfur content (wt%)**	**Initial discharge capacity**	**Capacity retention**			**Specific energy density (Wh kg^{-1})**	**Volumetric energy density (Wh L^{-1})**	**Ref**
		Capacity (mAh g_s^{-1})	Cycles	Retention rate (%)	Voltage window (V ver. Li/Li^+)			
Lepidocrocite titanium oxide/S*	**80**	**1024**	**300**	**82.3**	**1.7 ~ 2.7**	**1041.4**	**662.7**	**This work**
ACS70*	**70**	**1189**	**100**	**68.8**	**1.7~2.7**	**1054.9**	**667.6**	**This work**
CTAB-modified S–GO	~80	1440	1500	58.5	1.5~2.8	~500	-	20
CNT/sulfur	~90	789.3	85	~80	1.6~3.0	1249.2	-	21
S80/KB	80	~1000	100	~75	1.7~3.0	-	248	22,23
NG–CN sulfur	77	1000, 1100	-	-	1.7~2.8	-	476	22,24
S@MOFs/CNT	70	1263	500	60	1.7~2.8	-	663	22,25
GS-MWCNT@S	83	1396	100	60.5	1.0~3.0	513		26
VC/S75	75	-	100	52			1274	27

* Specific energy density is calculated by taking only electrodes into account based on n/p ratio of 1.5.

Table S4: The comparison of actual sulfur content in electrode between the **LTS80** and previous sulfur composites.

Material	Sulfur content (wt%)	Cathode composition (Active material : Conductive agent : Binder)	Cathode sulfur content (wt%)	Ref
Lepidocrocite-type titanium oxide nanosheet/S	**80**	**75:15:10**	**60**	**This work**
ACS70	**70**	**75:15:10**	**52.5**	**This work**
TiO_{2-x}@C-NP/S	70	80:10:10	56	28
B,N-doped TiO_2/S	68	80:10:10	54.4	29
TiO_{2-x}/sulfur	-	-	45	11
Sulphur–TiO_2 yolk–shell	72	75:15:10	53	12
$Ti_3C_2T_x$@Meso-C/S	72.88	80:10:10	58.30	30
S/VO_2-graphene	75	80:10:10	60	14
75S/MnO_2	75	75:15:10	56.25	13
Ti_2C/S	70	80:10:10	56	31
MnO_2 @HCF/S	71	70:20:10	49.7	32
CH@LDH/S	75	70:10:10:10	52.5	33
CNT/$NiFe_2O_4$-S	76	72:12:16	54.72	34
S-HMT@CNT	56	80:10:10	44.8	35
S/(CNT@MPC)	40	80:10:10	32	36
GS-MWCNT@S	70	70:20:10	49	26
Sulfur–carbon sphere composite	42	70:20:10	29.4	37

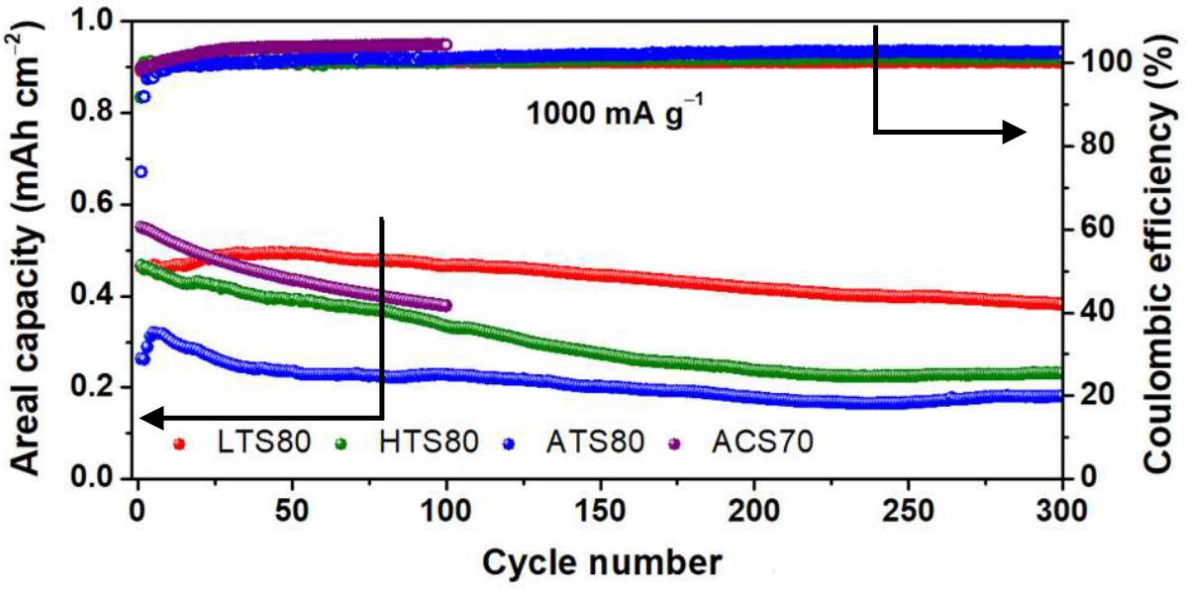

Figure S16. Areal capacity *vs* cycle number plots of **LTS80**, **HTS80**, **ATS80**, and its derivatives that contain commercial titanium oxide or carbon (**ACS70** at 0.8 mg cm^{-2}).

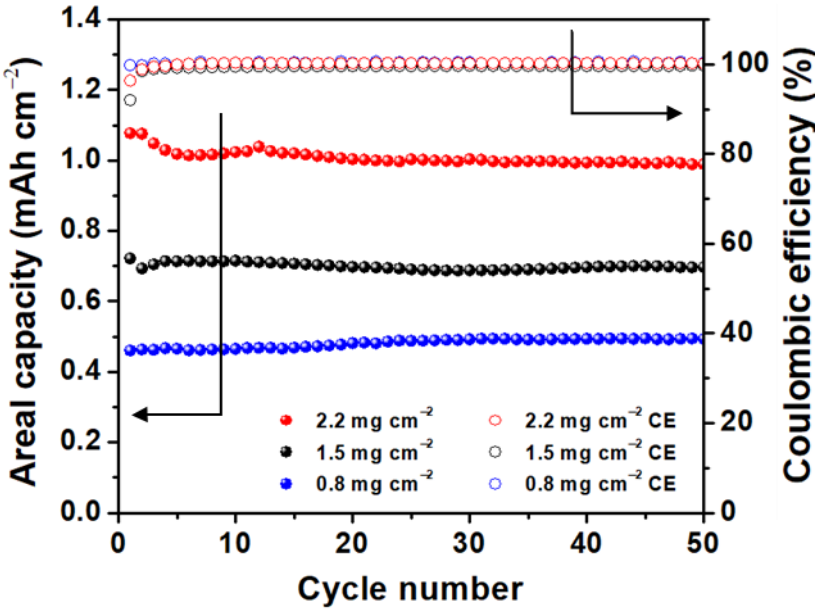

Figure S17. The areal capacities of **LTS80** with active loadings of 0.8, 1.5, and 2.2 mg cm^{-2}.

REFERENCES

(1) Sasaki, T.; Watanabe, M. Osmotic Swelling to Exfoliation. Exceptionally High Degrees of Hydration of a Layered Titanate. *J. Am. Chem. Soc*. **1998**, *120*, 4682-4689.

(2) Miyamoto, N.; Kuroda, K.; Ogawa, M. Exfoliation and Film Preparation of a Layered Titanate, $Na_2Ti_3O_7$, and Intercalation of Pseudoisocyanine Dye. *J. Mater. Chem*. **2004**, *14*, 165-170.

(3) Seo, J.; Jin, X.; Kim, M.; Kim, I. Y.; Jo, Y. K.; Bera, S.; Lee, N. S.; Lee, W. I.; Kim, H.; Hwang, S.-J. Exfoliated Metal Oxide Nanosheets as Effective and Applicable Substrates for Atomically Dispersed Metal Nanoparticles with Tailorable Functionalities. *Adv. Mater. Interfaces* **2016**, *3*, 1600661.

(4) Li, Z.-Q.; Chen, W.-C.; Guo, F.-L.; Mo, L.-E.; Hu, L.-H.; Dai, S.-Y. Mesoporous TiO_2 Yolk-Shell Microspheres for Dye-Sensitized Solar Cells with a High Efficiency Exceeding 11%. *Sci. Rep*. **2015**, *5*, 14178.

(5) Pang, Q.; Kundu, D.; Cuisinier, M.; Nazar, L. Surface-Enhanced Redox Chemistry of Polysulphides on a Metallic and Polar Host for Lithium-Sulphur Batteries. *Nat. Commun*. **2014**, *5*, 4759.

(6) Toby, B. H. EXPGUI, A Graphical User Interface for GSAS. *J. Appl. Crystallogr*. **2001**, *34*, 210-213.

(7) Rietveld, H. A Profile Refinement Method for Nuclear and Magnetic Structures. *J. Appl. Crystallogr*. **1969**, *2*, 65-71.

(8) Kresse, G.; Furthmüller J. Efficiency of ab-initio total energy calculations for metals and semiconductors using a plane-wave basis set. *Comput. Mater. Sci*. **1996**, *6*, 15-50.

(9) Perdew, J. P.; Burke, K.; Ernzerhof, M. Generalized Gradient Approximation Made Simple. *Phys. Rev. Lett*. **1996**, *77*, 3865.

(10) Evers, S.; Yim, T.; Nazar, L. F. Understanding the Nature of Absorption/Adsorption in Nanoporous Polysulfide Sorbents for the Li–S Battery. *J. Phys. Chem. C* **2012**, *116*, 19653-19658.

(11) Liang, Z.; Zheng, G.; Li, W.; Seh, Z. W.; Yao, H.; Yan, K.; Kong, D.; Cui, Y. Sulfur Cathodes with Hydrogen Reduced Titanium Dioxide Inverse Opal Structure. *ACS Nano* **2014**, *8*, 5249-5256.

(12) Seh, Z. W.; Li, W.; Cha, J. J.; Zheng, G.; Yang, Y.; McDowell, M. T.; Hsu, P.-C.; Cui, Y. Sulphur–TiO_2 Yolk–Shell Nanoarchitecture with Internal Void Space for Long-Cycle Lithium–Sulphur Batteries. *Nat. Commun*. **2013**, *4*, 1331.

(13) Liang, X.; Hart, C.; Pang, Q.; Garsuch, A.; Weiss, T.; Nazar, L. F. A Highly Efficient Polysulfide Mediator for Lithium–Sulfur Batteries. *Nat. Commun*. **2015**, *6*, 5682.

(14) Liang, X.; Kwok, C. Y.; Lodi-Marzano, F.; Pang, Q.; Cuisinier, M.; Huang, H.; Hart, C. J.; Houtarde, D.; Kaup, K.; Sommer, H., et al. Tuning Transition Metal Oxide–Sulfur Interactions for Long Life Lithium Sulfur Batteries: The "Goldilocks" Principle. *Adv. Energy Mater*. **2015**, *6*, 1501636.

(15) Zhang, Y.; Zhao, Y.; Yermukhambetova, A.; Bakenov, Z.; Chen, P. Ternary sulfur/polyacrylonitrile/$Mg_{0.6}Ni_{0.4}O$ composite cathodes for high performance lithium/sulfur batteries. *J. Mater. Chem. A* **2013**, *1*, 295-301.

(16) Ji, X.; Evers, S.; Black, R.; Nazar, L. F. Stabilizing Lithium–Sulphur Cathodes Using Polysulphide Reservoirs. *Nat. Commun*. **2011**, *2*, 325.

(17) Sun, F.; Wang, J.; Long, D.; Qiao, W.; Ling, L.; Lv, C.; Cai, R. A high-rate lithium–sulfur battery assisted by nitrogen-enriched mesoporous carbons decorated with ultrafine La_2O_3 nanoparticles. *J. Mater. Chem. A*, **2013**, *1*, 13283-13289.

(18) Yao, H.; Zheng, G.; Hsu, P.-C.; Kong, D.; Cha, J. J.; Li, W.; Seh, Z. W.; McDowell, M. T.; Yan, K.; Liang, Z., et al. Improving Lithium–Sulphur Batteries Through Spatial

Control of Sulphur Species Deposition on a Hybrid Electrode Surface. *Nat. Commun*. **2014**, *5*, 3943.

(19) Tao, Y.; Wei, Y.; Liu, Y.; Wang, J.; Qiao, W.; Ling, L.; Long, D. Kinetically-Enhanced Polysulfide Redox Reactions by Nb_2O_5 Nanocrystals for High-Rate Lithium–Sulfur Battery. *Energy Environ. Sci*. **2016**, 9, 3230-3239.

(20) Song, M.-K.; Zhang, Y.; Cairns, E. J. A Long-Life, High-Rate Lithium/Sulfur Cell: A Multifaceted Approach to Enhancing Cell Performance. *Nano Lett*. **2013**, *13*, 5891-5899.

(21) Cheng, X.-B.; Huang, J.-Q.; Zhang, Q.; Peng, H.-J.; Zhao, M.-Q.; Wei, F. Aligned carbon nanotube/sulfur composite cathodes with high sulfur content for lithium–sulfur batteries. *Nano Energy* **2014**, *4*, 65-72.

(22) Xue, W.; Miao, L.; Qie, L.; Wang, C.; Li, S.; Wang, J.; Li, J. Gravimetric and volumetric energy densities of lithium-sulfur batteries. *Curr. Opinion Electrochem*. **2017**, *6*, 92-99.

(23) Lv, D.; Zheng, J.; Li, Q.; Xie, X.; Ferrara, S.; Nie, Z.; Mehdi, L. B.; Browning, N. D.; Zhang, J.-G.; Graff, G. L., et al. High Energy Density Lithium–Sulfur Batteries: Challenges of Thick Sulfur Cathodes. *Adv. Energy Mater*. **2015**, *5*, 1402290

(24) Pang, Q.; Liang, X.; Kwok, C. Y.; Kulisch, J.; Nazar, L. F. A Comprehensive Approach toward Stable Lithium–Sulfur Batteries with High Volumetric Energy Density. *Adv. Energy Mater*. **2017**, *7*, 1601630

(25) Mao, Y.; Li, G.; Guo, Y.; Li, Z.; Liang, C.; Peng, X.; Lin, Z. Foldable interpenetrated metal-organic frameworks/carbon nanotubes thin film for lithium–sulfur batteries. *Nat. Commun*. **2017**, *8*, 14628.

(26) Chen, R. J.; Zhao, T.; Lu, J.; Wu, F.; Li, L.; Chen, J. Z.; Tan, G. Q.; Ye, Y. S.; Amine, K. Graphene-Based Three-Dimensional Hierarchical Sandwich-type Architecture for High-Performance Li/S Batteries. *Nano Lett*. **2013**, *13*, 4642-4649.

(27) Pang, Q.; Kundu, D.; Nazar, L. F. A Graphene-Like Metallic Cathode Host for Long-Life and High-Loading Lithium–Sulfur Batteries. *Mater. Horiz.* **2016**, *3*, 130-136.

(28) Li, Z.; Zhang, J.; Guan, B.; Wang, D.; Liu, L.-M.; Lou, X. W. D. A Sulfur Host Based on Titanium Monoxide@Carbon Hollow Spheres for Advanced Lithium–Sulfur Batteries. *Nat. Commun.* **2016**, *7*, 13065.

(29) Wang, X.; Gao, T.; Fan, X.; Han, F.; Wu, Y.; Zhang, Z.; Li, J.; Wang, C. Tailoring Surface Acidity of Metal Oxide for Better Polysulfide Entrapment in Li-S Batteries. *Adv. Funct. Mater.* **2016**, *26*, 7164-7169.

(30) Bao, W.; Su, D.; Zhang, W.; Guo, X.; Wang, G. 3D Metal Carbide@Mesoporous Carbon Hybrid Architecture as a New Polysulfide Reservoir for Lithium-Sulfur Batteries. *Adv. Funct. Mater.* **2016**, *26*, 8746-8756.

(31) Liang, X.; Garsuch, A.; Nazar, L. F. Sulfur Cathodes Based on Conductive MXene Nanosheets for High-Performance Lithium–Sulfur Batteries. *Angew. Chem. Int. Ed.* **2015**, 54, 3907-3911.

(32) Li, Z.; Zhang, J.; Lou, X. W. Hollow Carbon Nanofibers Filled with MnO_2 Nanosheets as Efficient Sulfur Hosts for Lithium–Sulfur Batteries. *Angew. Chem. Int. Ed.*, **2015**, *54*, 12886-12890.

(33) Zhang, J.; Hu, H.; Li, Z.; Lou, X. W. D. Double-Shelled Nanocages with Cobalt Hydroxide Inner Shell and Layered Double Hydroxides Outer Shell as High-Efficiency Polysulfide Mediator for Lithium–Sulfur Batteries. *Angew. Chem. Int. Ed.* **2016**, *55*, 3982-3986.

(34) Fan, Q.; Liu, W.; Weng, Z.; Sun, Y.; Wang, H. Ternary Hybrid Material for High-Performance Lithium–Sulfur Battery. *J. Am. Chem. Soc.* **2015**, *137*, 12946-12953.

(35) Hwang, J. Y.; Kim, H. M.; Lee, S. K.; Lee, J. H.; Abouimrane, A.; Khaleel, M. A.; Belharouak, I.; Manthiram, A.; Sun, Y. K. High-Energy, High-Rate, Lithium-Sulfur

Batteries: Synergetic Effect of Hollow TiO_2-Webbed Carbon Nanotubes and a Dual Functional Carbon-Paper Interlayer. *Adv. Energy Mater*. **2016**, *6*, 1501480.

(36) Xin, S.; Gu, L.; Zhao, N.-H.; Yin, Y.-X.; Zhou, L.-J.; Guo, Y.-G.; Wan, L.-J. Smaller Sulfur Molecules Promise Better Lithium–Sulfur Batteries. *J. Am. Chem. Soc*. **2012**, *134*, 18510-18513.

(37) Zhang, B.; Qin, X.; Li, G. R.; Gao, X. P. Enhancement of long stability of sulfur cathode by encapsulating sulfur into micropores of carbon spheres. *Energy Environ. Sci*. **2010**, *3*, 1531-1537.